Preparation and Multicolor Electrochromic Performance of a WO_3/Tris-(2,2′-bipyridine)ruthenium(II)/Polymer Hybrid Film

Masayuki Yagi,* Koji Sone, Miki Yamada, and Saori Umemiya[a]

Abstract: A tungsten trioxide (WO_3)/tris(2,2′-bipyridine)ruthenium(II) ($[Ru(bpy)_3]^{2+}$; bpy = 2,2′-bipyridine)/poly(sodium 4-styrenesulfonate) (PSS) hybrid film was prepared by electrodeposition from a colloidal triad solution containing peroxotungstic acid (PTA), $[Ru(bpy)_3]^{2+}$, and PSS. A binary solution of $[Ru(bpy)_3]^{2+}$ and PTA (30 vol% ethanol in water) gradually gave an orange precipitate, possibly caused by the electrostatic interaction between the cationic $[Ru(bpy)_3]^{2+}$ and the anionic PTA. The addition of PSS to the binary PTA/$[Ru(bpy)_3]^{2+}$ solution remarkably suppressed this precipitation and caused a stable, colloidal triad solution to form. The spectrophotometric measurements and lifetime analyses of the photoluminescence from the excited $[Ru(bpy)_3]^{2+}$ ion in the colloidal triad solution suggested that the $[Ru(bpy)_3]^{2+}$ ion is partially shielded from electrostatic interaction with anionic PTA by the anionic PSS polymer chain. The formation of the colloidal triad made the ternary $[Ru(bpy)_3]^{2+}$/PTA/PSS solution much more redox active. Consequently, the rate of electrodeposition of WO_3 from PTA increased appreciably by the formation of the colloidal triad, and fast electrodeposition is required for the unique preparation of this hybrid film. The absorption spectrum of the $[Ru(bpy)_3]^{2+}$ ion in the film was close to its spectrum in water, but the photoexcited state of the $[Ru(bpy)_3]^{2+}$ ion was found to be quenched completely by the presence of WO_3 in the hybrid film. The cyclic voltammogram (CV) of the hybrid film suggested that the $[Ru(bpy)_3]^{2+}$ ion performs as it is adsorbed onto WO_3 during the electrochemical oxidation. An ohmic contact between the $[Ru(bpy)_3]^{2+}$ ion and the WO_3 surface could allow the electrochemical reaction of adsorbed $[Ru(bpy)_3]^{2+}$. The composition of the hybrid film, analyzed by electron probe microanalysis (EPMA), suggested that the positive charge of the $[Ru(bpy)_3]^{2+}$ ion could be neutralized by partially reduced WO_3^- ions, in addition to Cl^- and PSS units, based on the charge balance in the film. The electrostatic interaction between the WO_3^- ion and the $[Ru(bpy)_3]^{2+}$ ion might be responsible for forming the electron transfer channel that causes the complete quenching of the photoexcited $[Ru(bpy)_3]^{2+}$ ion, as well as the formation of the ohmic contact between the $[Ru(bpy)_3]^{2+}$ ion and WO_3. A multicolor electrochromic performance of the WO_3/$[Ru(bpy)_3]^{2+}$/PSS hybrid film was observed, in which transmittances at 459 and 800 nm could be changed, either individually or at once, by the selection of a potential switch. Fast responses, of within a few seconds, to these potential switches were exhibited by the electrochromic hybrid film.

Keywords: electrochemistry · electrochromic material · hybrid film · ruthenium · tungsten trioxide

Introduction

There has been much interest in developing low-cost materials with multiple reflective or transmissive colors suitable for electronic devices, such as displays,[1,2] smart windows,[3,4] and electronic paper.[5,6] Electrochromic materials may be ideally suited to meet the needs of these emerging applications: they are cheap and simple to produce, and they can provide reasonable contrast in multiple colors.[6–8] Tungsten trioxide (WO_3) is a promising electrochromic material candidate for these devices, available at low-cost, with a simple procedure for film preparation.[9,10] Although WO_3 films can

[a] Prof. Dr. M. Yagi, K. Sone, M. Yamada, S. Umemiya
Faculty of Education and Human Sciences and Center for Transdisciplinary Research
Niigata University, 8050 Ikarashi-2
Niigata 950–2181 (Japan)
Fax: (+81) 25-262-7151
E-mail: yagi@ed.niigata-u.ac.jp

Supporting information for this article is available on the WWW under http://www.chemeurj.org/ or from the author. XRD data, an SEM image of a WO_3 film, and figures related to the influence of the hybridization of $[Ru(bpy)_3]^{2+}$ on the electrochromic performance of the WO_3/H_xWO_3 redox are available.

 DOI: 10.1002/chem.200400323

be prepared by several techniques, for example, vacuum evaporation,[11] chemical vapor deposition,[12] sol–gel precipitation,[13] spin-coating,[14] sputtering,[9] and electrodeposition,[15] simple and low-cost procedures should be selected for emerging applications.

Electrochemical reduction of a WO_3 film in an acidic solution yields a blue film of H_xWO_3, according to Equation (1).

$$WO_3 + xe^- + xH^+ \rightleftharpoons H_xWO_3 \quad (1)$$

H_xWO_3 has about 1/3 lower absorption in the range of ~400–500 nm relative to that at ~700–800 nm. Its hybridization with another electrochromic material, showing absorption in the ~400–500 nm range, could produce a promising electrochromic material with reasonable contrast in multiple colors. Tris(2,2′-bipyridine)ruthenium(II) ($[Ru(bpy)_3]^{2+}$) is a very stable compound with intense absorption in the metal-to-ligand charge-transfer (MLCT) band at 453 nm in aqueous solution, which is reversibly removed by oxidation to Ru^{III}. A bilayer of WO_3 and the $[Ru(bpy)_3]^{2+}$ ion dispersed in a polymer film could be a possible design for multicolor electrochromic devices. However, the charge transport rate in $[Ru(bpy)_3]^{2+}$-dispersed polymer films is not very fast because the charge transport in the films is basically diffusion-controlled (the apparent diffusion constant is $\sim 10^{-9}$–10^{-12} $cm^2 s^{-1}$).[16–18] We prepared a $WO_3/[Ru(bpy)_3]^{2+}$/PSS (PSS = poly(sodium 4-styrenesulfonate)) hybrid film by simple electrodeposition from a colloidal triad solution containing peroxotungstic acid (PTA), the $[Ru(bpy)_3]^{2+}$ ion, and PSS.[19] Herein, we report the formation of the colloidal triad solution, a unique preparation of a $WO_3/[Ru(bpy)_3]^{2+}$/PSS hybrid film, and its multicolor electrochromic performance with quick response times and high contrast.

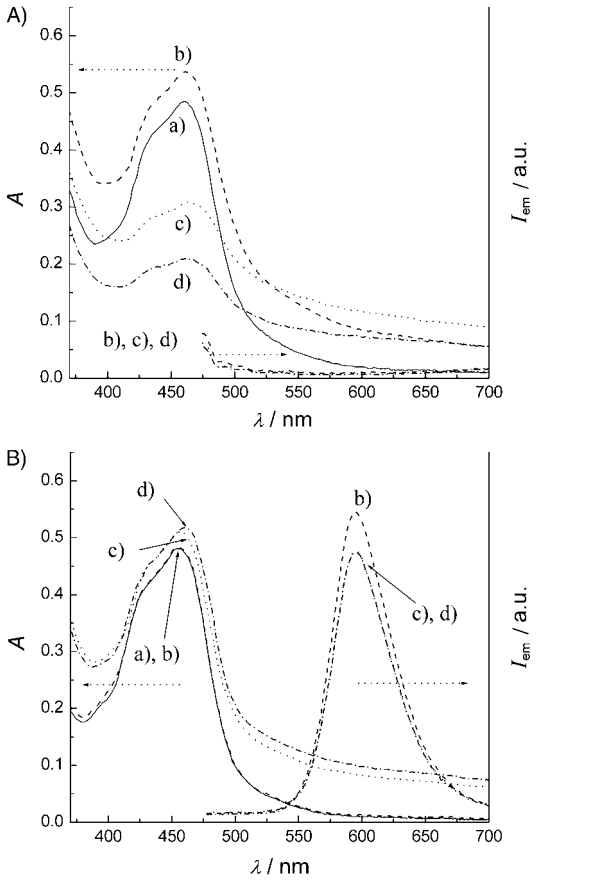

Figure 1. Absorption spectral change and emission spectral change (I_{em}: relative emission intensity) of a solution (30 vol% ethanol in water) containing 1 mM $[Ru(bpy)_3]^{2+}$ and 25 mM PTA: A) in the absence of PSS, and B) in the presence of 30 mM PSS. The solution was diluted by 30 times just before the measurements. The spectra were taken at a) 0, b) 20, c) 210, and d) 300 min aging time of the solution.

Results and Discussion

Investigation of a colloidal triad solution of $[Ru(bpy)_3]^{2+}$, PTA, and PSS: A binary solution of $[Ru(bpy)_3]^{2+}$ (1 mM) and PTA (25 mM) in a water/ethanol mix (30 vol% ethanol) gradually gave an orange precipitate, which is possibly formed by electrostatic interaction between the cationic $[Ru(bpy)_3]^{2+}$ and the anionic PTA. The addition of PSS to the binary PTA/$[Ru(bpy)_3]^{2+}$ solution suppressed this precipitation and resulted in a stable, colloidal triad solution. This is illustrated by the absorption spectral changes shown in Figure 1A and B. In the absence of PSS, the absorption spectrum of the binary solution just after preparation (absorption spectrum (a) at 0 min in Figure 1A) exhibited a maximum at $\lambda_{max} = 459$ nm, compared with $\lambda_{max} = 453$ nm for an aqueous $[Ru(bpy)_3]^{2+}$ solution. The absorbance at λ_{max} increased with time due to clouding of the solution, up to 20 min, and thereafter decreased due to the formation of the precipitate, giving an almost colorless solution at 300 min (Figure 1A, spectrum d). The MLCT-excited $[Ru(bpy)_3]^{2+}$ ion is known to emit intense phosphorescence at 590 nm in water at room temperature. In parallel with the absorption spectral measurement of the binary solution, a photoluminescence spectral change was also measured, but emission was not observed at all, as shown by the emission spectrum in Figure 1A. The solution did not emit even before the formation of the precipitate (at 20 min), showing that the photoexcited $[Ru(bpy)_3]^{2+}$ ion is completely quenched by the presence of PTA in the binary solution. This could be ascribed to the strong interaction between $[Ru(bpy)_3]^{2+}$ and PTA, most possibly by an electrostatic force. On the other hand, in the presence of PSS, the absorption spectra of the ternary solution ($[Ru(bpy)_3]^{2+}$, PTA, and PSS) gave absorption maxima at $\lambda_{max} = 454$ nm (Figure 1B). With increased aging time, the maximum absorbance slightly increased and shifted to 459 nm, at which it remained even after 300 min. Correspondingly, the photoluminescence spectra gave intense emission at $\lambda_{max} = 595$ nm, which slightly decreased in intensity at 210 min and then remained stable after 300 min (Figure 1B). This is in contrast to the complete quenching observed in the binary solutions.

To investigate the microscopic environment around the $[Ru(bpy)_3]^{2+}$ ions in the colloidal triad solution, the emis-

sion decay was measured to determine the lifetime (τ) of the photoexcited $[Ru(bpy)_3]^{2+}$ ions. The lifetime measurements are summarized in Table 1, which also includes the absorption and emission spectrophotometric data. A single-exponential fit of the emission decay of the excited $[Ru(bpy)_3]^{2+}$ ion in a water/ethanol (30 vol%) mix gave a lifetime of 560 ns at room temperature. The emission decay of a binary $[Ru(bpy)_3]^{2+}$/PSS solution was analyzed by means of a double-exponential fit, yielding a major long-lifetime component ($\tau_1 = 770$ ns, 87.3%) and a minor short-lifetime component ($\tau_2 = 119$ ns, 12.7%). The major long-lifetime component was 1.4 times longer than that of the $[Ru(bpy)_3]^{2+}$ ion in water/ethanol. This could be the result of a decrease in the nonradiative decay process by π–π interactions between the bpy ligands of $[Ru(bpy)_3]^{2+}$ and the 4-styrenesulfonate units of PSS.[20] The minor short-lifetime component could be generated by a concentration-quenching that occurs when complexes are concentrated in an anionic domain formed by PSS. The emission decay of the ternary $[Ru(bpy)_3]^{2+}$/PTA/PSS solution at an aging time of 20 min was also analyzed by a double-exponential fit, yielding a major long-lifetime component (786 ns, 85.3%) and a minor short-lifetime component (136 ns, 14.7%). The lifetimes and fractions of both the long- and short-lifetime components are close to those of the binary $[Ru(bpy)_3]^{2+}$/PSS solution. They did not change when the ternary solution turned into the colloidal triad solution after aging for 300 min. These results could suggest that the emitting $[Ru(bpy)_3]^{2+}$ ions are interacting with PSS by π–π and electrostatic interactions in the colloidal triad solution.

The relative emission yield (Φ_{rel}) of the $[Ru(bpy)_3]^{2+}$ ion in the colloidal triad solution at 300 min was 0.56 versus a value of 1.00 for the $[Ru(bpy)_3]^{2+}$ ion in the water/ethanol mixture. The former value was 42% of Φ_{rel} (1.32) for the binary $[Ru(bpy)_3]^{2+}$/PSS solution, implying that 42% of the $[Ru(bpy)_3]^{2+}$ complex content in the colloidal solution is emitting in the PSS domain. It can be concluded that $[Ru(bpy)_3]^{2+}$ ions are partially shielded from electrostatic interaction with PTA molecules by the anionic PSS polymer chain, suppressing precipitation in the ternary solution.

The formation of the colloidal triad can also be monitored by using a simple electrochemical technique. Figure 2 shows the cyclic voltammogram (CV) of the ternary $[Ru(bpy)_3]^{2+}$/PTA/PSS solution at different aging times. The CV taken at zero aging (Figure 2a) showed poor electrochemical reactivity in a reductive scan. As the aging time increased, the redox response at −0.5 V became clearly concomitant with the growth of the cathodic current below −0.8 V; the cause of this behavior can be assigned to reduction of PTA and/or protons.[21] The growth of the cathodic current was synchronous with the spectrophotometrically observable formation of the colloidal triad. The formation of the colloidal triad made the ternary $[Ru(bpy)_3]^{2+}$/PTA/PSS solution much more redox active. Possibly the $[Ru(bpy)_3]^{2+}$ ion prompts the aggregation of PTA, resulting in an increase of the redox potential of PTA to WO_3.

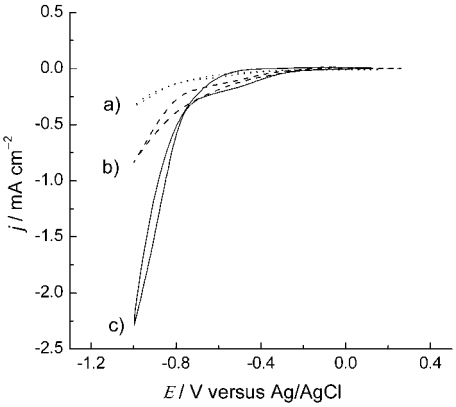

Figure 2. Change in the cyclic voltammogram of a ternary solution (1 mM $[Ru(bpy)_3]^{2+}$, 25 mM PTA, and 30 mM PSS) with aging time (a) 0, b) 175, and c) 330 min), measured at 100 mV s^{-1}. A four-day-old PTA solution was used.

The current densities at −1.0 V in the CVs of $[Ru(bpy)_3]^{2+}$/PTA/PSS solutions, prepared by using PTA solutions of different freshness, are plotted versus aging time in Figure 3, which includes the corresponding data for a PTA/PSS solution. The current density for the PTA/PSS solution did not change with aging time up until about 500 min, whereas the current density decreased for the $[Ru(bpy)_3]^{2+}$/PTA/PSS solutions, and reached around −2.0 to −2.5 mA cm^{-2} when the colloid was matured under the conditions employed. The decrease was observed over a shorter aging time when older PTA stock solutions were used (about 420, 300, and 120 min for one-, four-, and seven-day-old PTA, respectively). Thus, the formation of the $[Ru(bpy)_3]^{2+}$/PTA/PSS colloidal triad depended on the freshness of the PTA used.

Electrodeposition and characterization of a WO_3/$[Ru(bpy)_3]^{2+}$/PSS hybrid film: A WO_3/$[Ru(bpy)_3]^{2+}$/PSS hybrid film was successfully produced by a potentiostatic

Table 1. Summary of absorption and emission data of $[Ru(bpy)_3]^{2+}$ in various solutions at 25 °C.

System[a]	Aging time [min]	Absorption λ_{max}^{abs} [nm]	Emission λ_{max}^{em} [nm]	Φ_{rel}	τ_1 [ns]	(%)	τ_2 [ns]	(%)	Aspect
$[Ru(bpy)_3]^{2+}$/PTA/PSS	20	454	595	0.64	786	(85.3)	136	(14.7)	solution
	300	459	595	0.56	764	(84.6)	160	(15.4)	colloidal solution
$[Ru(bpy)_3]^{2+}$/PTA	20	459	n.e.[b]	0		n.e.			solution
$[Ru(bpy)_3]^{2+}$/PSS	20	453	595	1.32	770	(87.3)	119	(12.7)	solution
$[Ru(bpy)_3]^{2+}$	20	453	590	1.00	560	(100)			solution

[a] 30 vol% ethanol in water. The concentrations of $[Ru(bpy)_3]^{2+}$, PTA, and PSS are 0.033, 0.83, and 1.0 mM, respectively. [b] n.e. represents no emission.

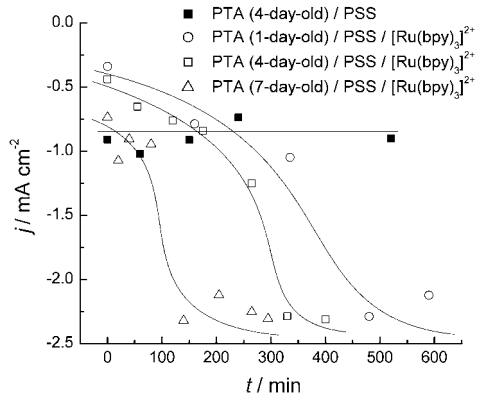

Figure 3. Plots of the current density (j) at -1.0 V for cyclic voltammograms of ternary $[Ru(bpy)_3]^{2+}$/PTA/PSS solutions, measured under the same conditions as shown in Figure 2. The solutions used are indicated in the legend.

electrodeposition (-0.45 V versus Ag/AgCl) from the colloidal triad solution of $[Ru(bpy)_3]^{2+}$/PTA/PSS. However, electrodeposition from the ternary solution, before the formation of the colloidal triad, did not yield a homogeneous hybrid film of sufficient thickness, showing that the formation of the colloidal triad is important for preparation of a homogeneous hybrid film. This can be explained by the kinetics of the electrodeposition. The current–time curves during the potentiostatic electrodeposition (up to $1.0\,C\,cm^{-2}$) from the ternary solution at different aging times are shown in Figure 4. The cathodic current densities

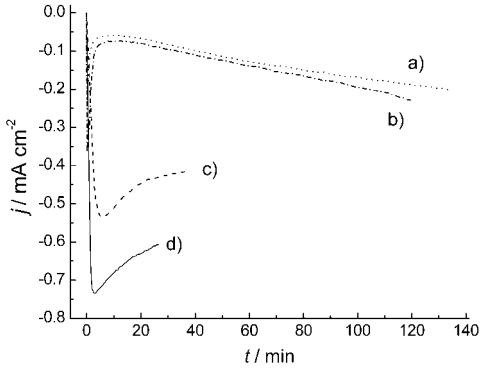

Figure 4. Current density–time curves during the electrodeposition of films from ternary solutions (1 mM $[Ru(bpy)_3]^{2+}$, 25 mM PTA, and 30 mM PSS) having different aging times of a) 0, b) 3, c) 8.5, and d) 10 h. The potentiostatic conditions were -0.45 V versus Ag/AgCl up to $1.0\,C\,cm^{-2}$.

for solutions aged for short times (0 and 3 h) are low (~ -0.059 to $-0.20\,mA\,cm^{-2}$ after aging for 3 h) relative to those for long-aged solutions (~ -0.61 to $-0.73\,mA\,cm^{-2}$ for 10 h-aging), in which the colloidal triad has formed. The fast electrochemical reduction of PTA to WO_3 could be required to incorporate the complex into the hybrid film.

The film thickness was measured by using scanning electron microscopic and interference spectroscopic techniques.[22] The plot of the film thickness versus the charge per unit area (Q in $C\,cm^{-2}$) applied during the electrodeposition is shown in Figure 5; it is a straight line with a slope of $0.56 \pm 0.024\,\mu m\,C^{-1}\,cm^2$, indicating that the film thickness is

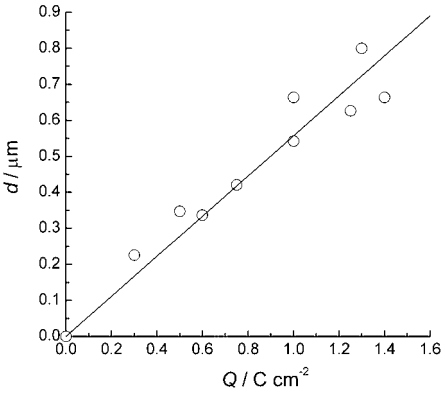

Figure 5. A plot of the film thickness (d) of $WO_3/[Ru(bpy)_3]^{2+}$/PSS hybrid films versus the amount of charge per unit area (Q) passed during electrodeposition under the conditions given for Figure 4.

easily controlled by Q. To check the uniformity of the film thickness, it was measured at different points in the film by means of a small monitoring spotlight (circle with roughly a 2 mm diameter). The thickness of the film (prepared by $1.0\,C\,cm^{-2}$ electrodeposition) was constant at $0.62 \pm 0.026\,\mu m$ at the different positions.

The visible absorption spectrum of the hybrid film exhibited a maximum at $\lambda_{max} = 459$ nm, based on the MLCT transition of $[Ru(bpy)_3]^{2+}$ (Figure 6a). This maximum is very close to that ($\lambda_{max} = 453$ nm) observed in water (Figure 6b). A plot of the absorbance at 459 nm versus Q gave a linear relationship (inset of Figure 6), showing no gradation of the confinement of $[Ru(bpy)_3]^{2+}$ ions in the film from the indium tin oxide (ITO)/film interface to the film surface.

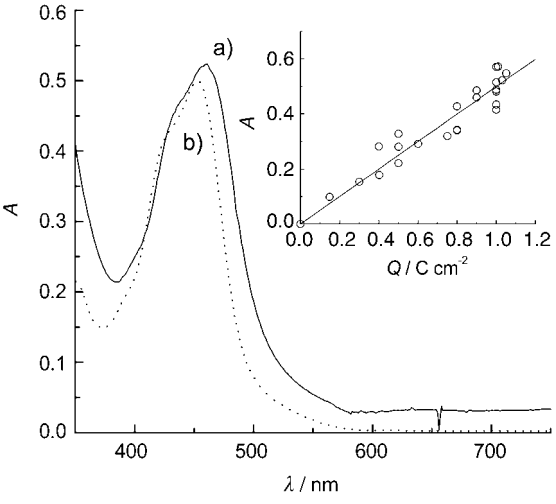

Figure 6. Absorption spectra of a) the $WO_3/[Ru(bpy)_3]^{2+}$/PSS hybrid film and b) $[Ru(bpy)_3]^{2+}$ in water. The inset shows the plot of absorbance at 459 nm versus Q, under the conditions given for Figure 4.

The coverage, Γ_{Ru} (in mol cm^{-2}), of $[Ru(bpy)_3]^{2+}$ ions on the electrode is related to the absorbance by the Lambert–Beer law: Absorbance $= \varepsilon\Gamma_{Ru} \times 10^3$, where ε (in M^{-1}cm^{-1}) is the molecular absorption coefficient of $[Ru(bpy)_3]^{2+}$ in the hybrid film at 459 nm. The slope (0.50 ± 0.04 C^{-1}cm^2) of the line provides $\Gamma_{Ru}/Q = 3.4 \times 10^{-8}$ mol C^{-1}, assuming ε of $[Ru(bpy)_3]^{2+}$ in water is 14600 M^{-1}cm^{-1} at $\lambda_{max} = 453$ nm.

The photoluminescence spectrum of the hybrid film was measured at the 459 nm excitation, but emission was not detected at all in the range of ~500–800 nm, in contrast to the intense photoluminescence at 590 nm observed in water. The photoanodic current generated at the rest potential (0.4 V versus the saturated calomel reference electrode, SCE) by visible light irradiation indicated that the quenching of photoexcited $[Ru(bpy)_3]^{2+}$ ions occurs by means of an oxidative mechanism by a WO_3 matrix.[19] Such efficient quenching was not caused by a simple physical adsorption of the $[Ru(bpy)_3]^{2+}$ ion onto WO_3 particles.[19] This result implies that there is some interaction between $[Ru(bpy)_3]^{2+}$ and WO_3 causing an electron transfer channel to form from the excited state, possibly to a conduction band of WO_3.

A WO_3 film on an ITO electrode gave a typical n-type semiconductor CV, in which any redox wave was not observed above 0.26 V of its flat band (FB) potential (Figure 7a). The redox below 0.26 V is based on H_xWO_3/WO_3

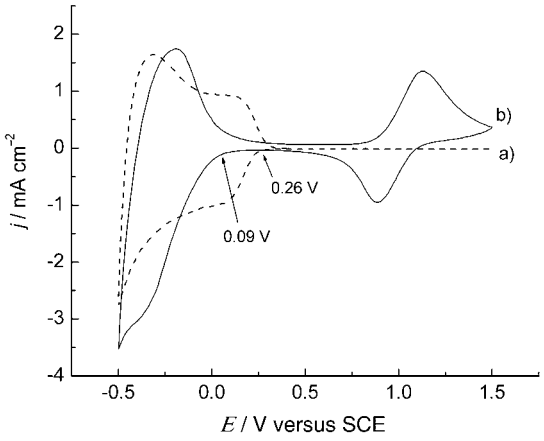

Figure 7. Cyclic voltammograms of a) a WO_3 film and b) a WO_3/$[Ru(bpy)_3]^{2+}$/PSS hybrid film, both dipped in a 0.1 M KNO_3 aqueous solution (pH 1.2) and measured at 100 mV s^{-1}.

with an electrochromic performance of blue/colorless. A CV of the WO_3/$[Ru(bpy)_3]^{2+}$/PSS film on an ITO electrode exhibited a reversible redox wave at 1.03 V on a Ru^{II}/Ru^{III} redox, which is nearly equal to its redox potential (1.06 V) measured in aqueous solution, in addition to the redox wave of H_xWO_3/WO_3 (Figure 7b). The potential at the initial rise of cathodic current on the reduction of WO_3 to H_xWO_3, shifted from 0.26 to 0.09 V by hybridization with the $[Ru(bpy)_3]^{2+}$ ion. As for the potential shift, a possible explanation could be that the over-potential for the reduction of WO_3 increases by some kinetic factor. However, the cathodic current at −0.5 V was larger (faster reduction) than that for the WO_3 film, which does not suggest an over-potential increase by some kinetic factor. Another explanation is the shift of the FB potential of WO_3 by interaction with $[Ru(bpy)_3]^{2+}$. To evaluate this FB potential shift, the redox response (redox potential = 0.16 V) between Prussian Blue (PB: ferric ferrocyanide, Fe^{II}–Fe^{III}) and Prussian White (PW: Fe^{II}–Fe^{II}) was investigated on the WO_3 film or the WO_3/$[Ru(bpy)_3]^{2+}$/PSS hybrid film. The CV of the WO_3/PB bilayer film-coated electrode exhibited a clear redox wave between PB and PW at 0.16 V, but the CV of the (WO_3/$[Ru(bpy)_3]^{2+}$/PSS)/PB bilayer-coated electrode did not exhibit this at all.[23] This result demonstrated that the redox between PB and PW is disturbed by the WO_3/$[Ru(bpy)_3]^{2+}$/PSS, but not by the WO_3 base layer. The hybridization of WO_3 with $[Ru(bpy)_3]^{2+}$ is considered to shift down the FB potential of WO_3 (0.26 to 0.09 V), preventing the electrochemical reduction of PB.

The anodic peak current at 1.03 V, due to Ru^{II}/Ru^{III} in the hybrid film, increased linearly with the scan rate, v (in V s^{-1}), not with $v^{1/2}$, in the range of ~5–100 mV s^{-1}. This shows that the $[Ru(bpy)_3]^{2+}$ ion performs as it is adsorbed on the WO_3 surface during the electrochemical reaction in the film. An ohmic contact between $[Ru(bpy)_3]^{2+}$ ions and the WO_3 surface could allow the electrochemical reaction of adsorbed $[Ru(bpy)_3]^{2+}$ ions. The slope of the straight line gave a coverage on the electrode of $\Gamma_{Ru} = 1.3 \times 10^{-8}$ mol cm^{-2}, based on the equation, $i_p = n^2F^2Av\Gamma_{Ru}/4RT$, where i_p, n, F, A, R, and T are the peak current (in A), number of electrons, Faraday constant, electrode area (1 cm^2), gas constant, and temperature (298 K), respectively. This value of Γ_{Ru} was identical to that calculated from absorbance data, showing that the fraction of the electroactive complex is nearly 100% in the CV measurements.

The X-ray diffraction (XRD) spectra of the WO_3/$[Ru(bpy)_3]^{2+}$/PSS hybrid film and the WO_3 film were measured. In neither of these XRD patterns was a peak for any crystalline WO_3 observed, aside from a very weak peak for the ITO substrate. This shows that amorphous WO_3 exists in the hybrid and WO_3 films. However, when these films were sintered at 550 °C, X-ray peaks due to crystalline phases were detected at $2\theta(°) = 11.0$, 22.0, 23.3, 23.7, 24.5 and 33.1 (see Figure S1 in the Supporting Information).

Scanning electron microscopy (SEM) was used to see the morphological features of the hybrid film. The ×500 image at the bulk surface of the hybrid film displays a homogeneous morph (Figure 8a), and the magnified image of this shows the WO_3 particles with ~150–500 nm diameter (Figure 8b). A significant clue to reveal the mode of electrodeposition of the hybrid film was found when the surface near the film-edge was observed. The SEM image of this edge surface displayed the film growing along the film surface (Figure 8c). This mode of growth can lead to a lamination layer structure of the film (Figure 8d). This lamination layer structure can be observed in WO_3 films prepared from either a 25 mM PTA solution or a 25 mM PTA/30 mM PSS solution (see Figures S2 and S3 in the Supporting Informa-

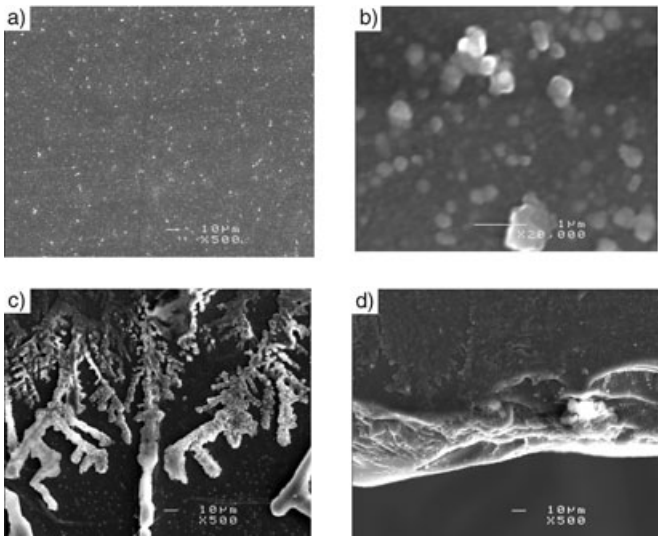

Figure 8. SEM images of a $WO_3/[Ru(bpy)_3]^{2+}$/PSS hybrid film. a) Bulk surface (×500, scale bar 10 μm), b) magnified bulk surface (×20000, scale bar 1 μm), c) surface near edge (×500, scale bar 10 μm), and d) surface at edge (×500, scale bar 10 μm).

tion), showing that the electrodeposition of WO_3 from the PTA solution yields the structure regardless of the presence of PSS under the conditions employed.

The local element analysis on the film surface was conducted by an EPMA technique. A wavelength-dispersive characteristic X-ray (WDX) spectrum of the $WO_3/[Ru(bpy)_3]^{2+}$/PSS hybrid film revealed peaks due to elements W, Ru, and Cl[24] from their λ_{max} values, in addition to peaks due to In and Sn (originating from the ITO substrate), as shown in Figure 9A. The assignment of the peak at 5.37 Å is somewhat unclear, and it could possibly be due to either a Kα band for S or to some minor band for W. This assignment is crucial, because the presence of an S element signal is evidence of the presence of PSS in the film and possibly a measure of the local content of PSS. To identify the peak at 5.37 Å, the WDX spectrum of the hybrid film was measured carefully from 5.2 to 5.6 Å with a higher resolution. It exhibited two distinguishable peaks at 5.35 and 5.37 Å (Figure 9B), and was reasonably deconvoluted to two Gaussian bands that are shown by dotted lines in spectrum a; one is a broad band with $\lambda_{max}=5.347$ Å and a half bandwidth $\lambda_{1/2}=0.042$ Å, and the other is a sharp band with $\lambda_{max}=5.368$ Å and $\lambda_{1/2}=0.009$ Å. These broad and sharp bands were assigned to the elements W and S by comparison with λ_{max} and $\lambda_{1/2}$ for W and S standards, as shown in spectra b and c of Figure 9B, respectively. For the W and S standards, $\lambda_{max}=5.349$ Å, $\lambda_{1/2}=0.041$ Å, and $\lambda_{max}=5.371$ Å, $\lambda_{1/2}=0.010$ Å, respectively. The mapping measurement of S on the film surface, based on the Kα band for S at 5.368 Å, revealed that S was homogeneously distributed in the film. These results corroborate the fact that PSS is homogeneously incorporated in the hybrid film.

The deconvolution of a Kα band for S from the WDX spectrum allowed elemental analysis to be carried out. The

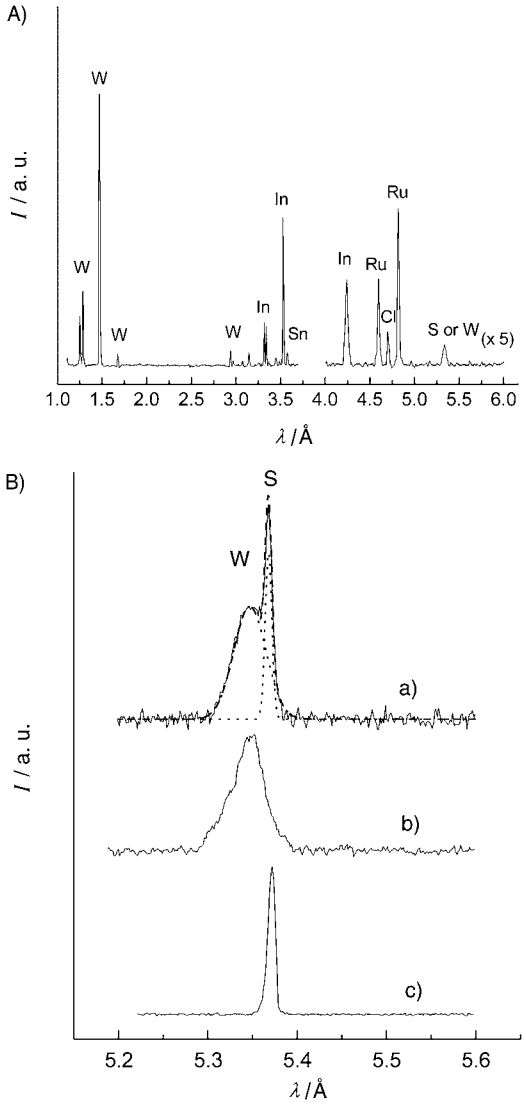

Figure 9. A) A wavelength dispersive characteristic X-ray (WDX) spectrum (I: Intensity) of the $WO_3/[Ru(bpy)_3]^{2+}$/PSS hybrid film. The spectrum between 4.0 and 6.0 Å was scaled up five times in intensity. B) A highly resolved WDX spectrum in the range of ~5.2–5.6 Å of a) the $WO_3/[Ru(bpy)_3]^{2+}$/PSS hybrid film, b) a tungsten standard, and c) a sulfur standard. In a), the dotted curves are deconvoluted Gaussian bands, and the dashed line is a simulation spectrum. The Gaussian bands were deconvoluted by using the converted energy dispersive spectrum.

molar ratio of W:Ru:Cl:S was 130:6.2:0.31:1. This was given from the intensity ratio of Lα bands of W and Ru, at 1.48 and 4.85 Å, respectively, a Kα band of Cl at 4.73 Å, and a deconvoluted Kα band of S at 5.368 Å. The elemental analysis indicated that there was a higher content of cationic $[Ru(bpy)_3]^{2+}$ than the sum of the contents of anionic Cl^- and PSS units, even when the peak intensity error is considered. The positive charge of the $[Ru(bpy)_3]^{2+}$ ions must be compensated by some sort of anionic species, to account for charge balance in the hybrid film. The positive charge of the $[Ru(bpy)_3]^{2+}$ ion could be neutralized by a partially reduced WO_3^- ion that could be stabilized by electrostatic interac-

tion with the $[Ru(bpy)_3]^{2+}$ ions in the film. This electrostatic interaction might be responsible for the electron transfer channel that causes the complete quenching of the photoexcited $[Ru(bpy)_3]^{2+}$ ion, as well as the formation of the ohmic contact between the $[Ru(bpy)_3]^{2+}$ ion and WO_3.

Multicolor electrochromic performance of the WO_3/$[Ru(bpy)_3]^{2+}$/PSS hybrid film: The multicolor electrochromic performance of the WO_3/$[Ru(bpy)_3]^{2+}$/PSS hybrid film is shown by the transmittance spectra in Figure 10. Under

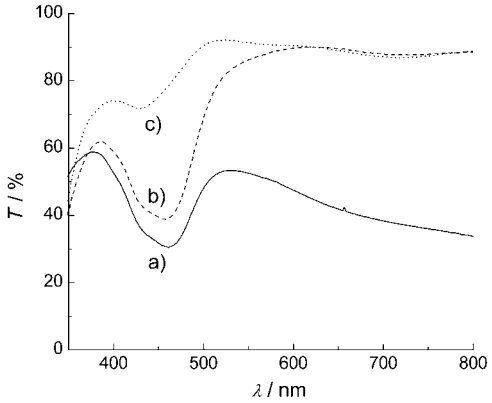

Figure 10. Transmittance spectra of the WO_3/$[Ru(bpy)_3]^{2+}$/PSS hybrid film on applying potentials of a) −0.5 V, b) 0.4 V, or c) 1.5 V, versus SCE.

an applied potential of −0.5 V, the color of the film was green with low transmittance (T) values of 30 and 33% at 459 and 800 nm, responsible for absorptions by $[Ru(bpy)_3]^{2+}$ and H_xWO_3, respectively. On applying 0.4 V, T at wavelengths greater than 550 nm increased to more than 86% due to oxidation of H_xWO_3 to WO_3, giving a yellow film. In a successive potential switch to 1.5 V, T at 459 nm increased to 78%, resulting in a colorless film. Figure 11 shows the T

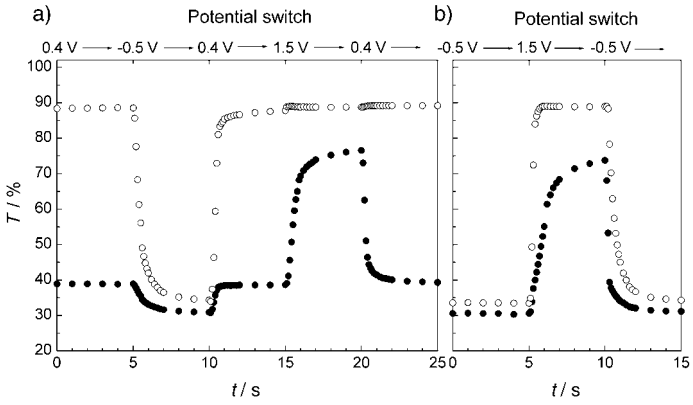

Figure 11. The transmittance change of the WO_3/$[Ru(bpy)_3]^{2+}$/PSS hybrid film by potential switches of 0.4 V→−0.5 V→0.4 V→1.5 V→0.4 V (a), and −0.5 V→1.5 V→−0.5 V (b). Full and open circles are transmittance changes at 459 and 800 nm, respectively.

changes caused by switching the applied potential in a dual-wavelength mode of 459 and 800 nm. The transmittance at 800 nm decreased from 89 to 34% with a potential switch from 0.4 to −0.5 V, and reversed back to the original T value by switching the potential back to 0.4 V (Figure 11a). Although T at 459 nm underwent an 8% change during this potential switch due to an absorption tail of H_xWO_3, this change was very low relative to that at 800 nm (55%). Conversely, T at 459 nm increased from 39 to 77% by a potential switch from 0.4 to 1.5 V, and was returned to the original T value by switching back to 0.4 V, while there was no change in the T value at 800 nm during these switches (Figure 11a). Thus, the transmittance values at 459 and 800 nm can be individually changed by potential switches. Simultaneous and reversible changes in T at 459 and 800 nm can be caused by a potential switch between −0.5 V and 1.5 V (Figure 11b). The quick response (less than a few seconds) of each change in transmittance was demonstrated. These fast-response changes in transmittance in the dual-wavelength mode are the special features of this WO_3/$[Ru(bpy)_3]^{2+}$/PSS hybrid film. Such performance characteristics can not be obtained by using an additive combination of a WO_3 film and $[Ru(bpy)_3]^{2+}$-dispersed solid films.

Preliminary, potential-step chronoamperometric measurements for the hybrid film revealed very fast charge transport by oxidation of Ru^{II} to Ru^{III}, with an apparent diffusion constant (D_{app}) of ~1.5–3.2×10^{-7} cm^2s^{-1}, depending on the terminal potential, in the potential step from 0.4 V (initial potential) to ~1.3–1.8 V (terminal potential). The D_{app} values are two to five orders of magnitude higher than those in $[Ru(bpy)_3]^{2+}$/polymer films (~10^{-9}–10^{-12} cm^2s^{-1}),[16–18] which are well studied as electrochromic films under the comparative conditions of 1 μm film thickness and 2.3×10^{-8} mol of $[Ru(bpy)_3]^{2+}$ ion coverage. In $[Ru(bpy)_3]^{2+}$/polymer films, charge transport is basically diffusion-controlled, and D_{app} is, in principle, independent of the terminal potential if it is sufficiently higher than the redox potential of Ru^{II}/Ru^{III}. This result implies a specific mechanism of charge transport in the hybrid film, detailed studies on which will be reported elsewhere.[25]

Conclusion

The preparation of a WO_3/$[Ru(bpy)_3]^{2+}$/PSS hybrid film was reported. It was formed by simple electrodeposition on an ITO electrode from a colloidal triad solution containing peroxotungstic acid, $[Ru(bpy)_3]^{2+}$, and PSS. The formation of the colloidal triad solution was investigated in detail by using UV/Vis absorption, emission spectroscopic, and electrochemical techniques. PSS suppressed the precipitation that is possibly caused by the cationic $[Ru(bpy)_3]^{2+}$ and anionic PTA, to give a stable, colloidal triad solution. The hybrid film was characterized by using UV/Vis absorption, spectroscopic, electrochemical, scanning electron microscopic, and electron probe microanalysis techniques. The hybrid film demonstrated a quick response in its multicolor electro-

chromic performance. The hybrid film is expected, as a multicolor electrochromic material, to find application in electronic devices such as displays, smart windows, and electronic papers. The preparation technique could initiate production of a wide range of WO_3-based films, hybridized with functional molecules and polymers.

Experimental Section

Materials: $[Ru(bpy)_3]Cl_2 \cdot 6H_2O$ and PSS (MW = 70000) were purchased from Aldrich Chemical Co., Inc. and used as-received. Tungsten powder and hydrogen peroxide (30%) were purchased from Kanto Kagaku Co., Ltd.

Preparations:*Preparation of the colloidal triad solution of $[Ru(bpy)_3]^{2+}$, PTA, and PSS*: In the preparation of a PTA solution, tungsten powder (0.92 g, 5.0 mmol) was dissolved in the hydrogen peroxide solution (30%), and then excess hydrogen peroxide was decomposed by Pt black. Ethanol was added to stabilize the PTA solution, finally giving a water/ethanol mixture (30 vol% ethanol) containing 50 mM PTA.[26] This solution was used as a stock solution. $[Ru(bpy)_3]^{2+}$ and PSS solutions were added to this PTA stock solution to prepare a solution containing 1 mM $[Ru(bpy)_3]^{2+}$, 25 mM PTA, and 30 mM PSS. After standing the solution at room temperature, it turned into a colloidal triad solution of $[Ru(bpy)_3]^{2+}$, PTA, and PSS. The standing time depended on the freshness of the PTA stock solution. More than 10 h were needed to give the colloidal triad solution if very fresh PTA stock solution (several hours old) was used, whereas 5 h were needed if four-day-old PTA solution was used. However, two-week-old PTA solution no longer produced a colloidal triad solution, but rather led immediately to precipitation.

Preparation of the WO_3/$[Ru(bpy)_3]^{2+}$/PSS hybrid film: A conventional, single-compartment electrochemical cell was equipped with an ITO working electrode, an Ag/AgCl reference electrode, and a platinum wire counter electrode for the electrodeposition. Typically, the WO_3/$[Ru(bpy)_3]^{2+}$/PSS hybrid film was electrodeposited from the colloidal triad solution (1 mM $[Ru(bpy)_3]^{2+}$, 25 mM PTA, and 30 mM PSS), with stirring, on an ITO electrode under the potentiostatic conditions: -0.45 V versus Ag/AgCl, up to 1.0 C cm^{-2}. The hybrid film was cathodically polarized at -0.5 V versus SCE in a 0.1 M HNO_3 aqueous solution, to complete the electrodeposition of PTA. As a comparison, a WO_3 film was prepared on an ITO electrode under the same conditions from a water/ethanol mix (30 vol% ethanol) containing 25 mM PTA and 30 mM PSS.

Measurements: For spectrophotometrical measurements, the colloidal triad solution was diluted by 30 times just before the measurement was taken, to gain a spectroscopically analyzable spectrum. UV/Vis absorption and emission spectra were measured by a photodiode-array spectrophotometer (Shimadzu, Multispec-1500) and a fluorescence spectrometer (Hitachi F-4010), respectively. The lifetime of the photoexcited $[Ru(bpy)_3]^{2+}$ ion was analyzed from the phosphorescence decay at 590 nm, measured by a time-correlated, single-photon counting apparatus (IBH, 5000F), equipped with a nanoflash lamp. To measure the film thickness, a spectrophotometer with a charge-coupled device (CCD) (Lambda vision, SA-100) and film thickness analysis software (Lambda vision, TF-Lab) were used. X-ray diffraction (MAC Science, MX labo), scanning electron microscopy (JEOL, JSM-6400), and electron probe microanalysis (Shimadzu, EPMA-8750) characterization techniques were used. Cyclic voltammograms were measured by using a single-compartment electrochemical cell equipped with an ITO, or the hybrid film-coated ITO working electrode, an Ag/AgCl or SCE reference electrode, and a platinum wire counter electrode. All the electrochemical experiments were carried out under an argon atmosphere by using an electrochemical analyzer (Hokuto Denko, HZ-3000). Spectroelectrochemical measurements were conducted by combining the photodiode array spectrophotometer with the electrochemical analyzer.

Acknowledgement

We thank Mr. A. Yanagisawa (Faculty of Engineering, Niigata University) for help with SEM measurements and Dr. M. Kobayashi (Center for Instrument Analysis, Niigata University) for help with EPMA measurements. Research was partially supported by a Toray Science and Technology Grant and a Grant for Promotion of Niigata University Research Projects.

[1] C. Bechinger, S. Ferrer, A. Zaban, J. Sprague, B. A. Gregg, *Nature* **1996**, *383*, 608–610.
[2] H. W. Heuer, R. Wehrmann, S. Kirchmeyer, *Adv. Funct. Mater.* **2002**, *12*, 89–94.
[3] M. Nagasu, N. Koshida, *J. Appl. Phys.* **1992**, *71*, 398–402.
[4] R. D. Rauh, *Electrochim. Acta* **1999**, *44*, 3165–3176.
[5] J. A. Rogers, *Science* **2001**, *291*, 1502–1503.
[6] U. Bach, D. Corr, D. Lupo, F. Pichot, M. Ryan, *Adv. Mater.* **2002**, *14*, 845–848.
[7] R. J. Mortimer, *Chem. Soc. Rev.* **1997**, *26*, 147–156.
[8] D. R. Rosseinsky, R. J. Mortimer, *Adv. Mater.* **2001**, *13*, 783–793.
[9] D. L. Bellac, A. Azens, C. G. Granqvist, *Appl. Phys. Lett.* **1995**, *66*, 1715–1716.
[10] S.-H. Baeck, K.-S. Choi, T. F. Jaramillo, G. D. Stucky, E. W. McFarland, *Adv. Mater.* **2003**, *15*, 1269–1273.
[11] R. J. Colton, A. M. Guzman, J. W. Rabalais, *J. Appl. Phys.* **1978**, *49*, 409–416.
[12] B. Yous, S. Robin, A. Donnadieu, G. Dufour, C. Maillot, H. Roulet, C. Senemaud, *Mater. Res. Bull.* **1984**, *19*, 1349–1354.
[13] C. Santato, M. Odziemkowski, M. Ulmann, J. Augustynski, *J. Am. Chem. Soc.* **2001**, *123*, 10639–10649.
[14] K. Yamanaka, H. Oakamoto, H. Kidou, T. Kudo, *Jpn. J. Appl. Phys., Part 1* **1986**, *25*, 1420–1426.
[15] P. K. Shen, A. C. C. Tseung, *J. Mater. Chem.* **1992**, *2*, 1141–1147.
[16] R. W. Murray in *Molecular Design of Electrode Surface*, *Vol. 22*, (Ed. W. H. J. Saunders), Wiley, New York, **1992**.
[17] M. Yagi, T. Mitsumoto, M. Kaneko, *J. Electroanal. Chem.* **1997**, *437*, 219–223.
[18] M. Yagi, T. Mitsumoto, M. Kaneko, *J. Electroanal. Chem.* **1998**, *448*, 131–137.
[19] M. Yagi, S. Umemiya, *J. Phys. Chem. B* **2002**, *106*, 6355–6357.
[20] Y. Kurimura, H. Yokota, K. Shigehara, E. Tsuchida, *Bull. Chem. Soc. Jpn.* **1982**, *55*, 55–58.
[21] The proton reduction might possibly be catalyzed by either WO_3, PTA, or species of PTA aggregated by the $[Ru(bpy)_3]^{2+}$ ion.
[22] The thin hybrid film yielded interference on a visible reflectance spectrum. When the monitor light was incident perpendicular to the film surface, and the vertically reflected light was detected, the optical film thickness, d_{opt} (in nm), is given by the following equation (see references [27]–[29]): $d_{opt} = nd = \lambda_{2m}\lambda_{2m+1}/(4(\lambda_{2m}-\lambda_{2m+1}))$, where n and d are refractive index and absolute film thickness (in nm), respectively, and λ_{2m} and λ_{2m+1} are the maximum and minimum wavelengths (in nm) on the interference spectrum, respectively. λ_{2m} and λ_{2m+1} were calculated from interference spectral data, by means of film thickness analysis software (Lambda vision, TF-Lab) to provide d_{opt}. The comparison of d_{opt} (1.06 μm) with d (0.55 μm, measured by an SEM technique) of the hybrid film, prepared by 1.0 C cm^{-2} electrodeposition, gave $n = 1.9$, which is close to the WO_3 crystal refractive index (2.2 (at 550 nm)) reported in the literature (see Ref. [27]). The d_{opt} values were measured for the various hybrid films at different Q, and d values were given from the d_{opt} values and $n = 1.9$.
[23] WO_3/PB and (WO_3/$[Ru(bpy)_3]^{2+}$/PSS)/PB bilayer electrodes were prepared as follows: a PB film was cathodically electrodeposited on a WO_3 film or a WO_3/$[Ru(bpy)_3]^{2+}$/PSS film from a colloidal solution containing 10 mM $FeCl_3$ and 10 mM $K_3[Fe(CN)_6]$ under galvanostatic conditions of -0.2 mA cm^{-2}.
[24] The Cl element originates from the counteranion of the $[Ru(bpy)_3]Cl_2$ salt.
[25] M. Yagi, K. Sone, M. Yamada, unpublished results.

[26] 100 mM with respect to W concentration; the structure of PTA in an aqueous solution is reported to be $[(O_2)_2(O)W{\cdot}O{\cdot}W(O)(O_2)_2]^{2-}$ (see references [14] and [15]).
[27] C.-C. Lee, *Optical Thin Film and Coating Technologies*, ULVAC, Tokyo, **2002**.
[28] R. Swanepoel, *J. Phys. E: Sci. Instrum.* **1983**, *16*, 1214–1222.
[29] J. C. Manifacier, J. Gasiot, J. P. Fillard, *J. Phys. E: Sci. Instrum.* **1976**, *9*, 1002–1004.

Received: April 1, 2004
Revised: June 22, 2004
Published online: November 17, 2004

